

## AUTOMATED DATA ANALYSIS FOR CONSECUTIVE IMAGES FROM DROPLET COMBUSTION EXPERIMENTS

CHRISTOPHER L DEMBIA<sup>✉</sup>, YU-CHENG LIU AND C. THOMAS AVEDISIAN

Sibley School of Mechanical and Aerospace Engineering, Cornell University, Ithaca, NY 14853-7501, USA  
e-mail: cld72@cornell.edu; yl677@cornell.edu; cta2@cornell.edu

(Received March 7, 2012; revised July 11, 2012; accepted August 8, 2012)

### ABSTRACT

A simple automated image analysis algorithm has been developed that processes consecutive images from high speed, high resolution digital images of burning fuel droplets. The droplets burn under conditions that promote spherical symmetry. The algorithm performs the tasks of edge detection of the droplet's boundary using a grayscale intensity threshold, and shape fitting either a circle or ellipse to the droplet's boundary. The results are compared to manual measurements of droplet diameters done with commercial software. Results show that it is possible to automate data analysis for consecutive droplet burning images even in the presence of a significant amount of noise from soot formation. An adaptive grayscale intensity threshold provides the ability to extract droplet diameters for the wide range of noise encountered. In instances where soot blocks portions of the droplet, the algorithm manages to provide accurate measurements if a circle fit is used instead of an ellipse fit, as an ellipse can be too accommodating to the disturbance.

Keywords: circle fitting, droplet combustion, edge detection, image analysis, least squares.

### INTRODUCTION

Extracting physical dimensions from consecutive digital images of a transient event is a fundamental problem in image analysis. This task is especially important in the study of droplet combustion in which droplet and flame diameter histories are determined from analyses of consecutive digital images. Such data provide the rate of combustion that relates to the performance of practical liquid-fueled propulsion systems. The data analysis problem for droplet burning is often complicated by the formation of soot around the droplet that introduces background noise that must be filtered out in order to ensure accurate diameter measurements. Individual images may be analyzed by manual processes using commercial software that require subjective judgments about which regions to omit from an image. Several hundreds of consecutive frames from high speed imaging devices (film and video) must typically be analyzed individually to extract the droplet diameter history, which can be time-intensive. For example, the time to manually analyze between 50 and 100 frames typically takes several hours. A process that could reduce the analysis would significantly improve the efficiency of data analysis and allow for study of a wider range of fuel systems within a specified period of time.

The ability to use planar images, which provide only two-dimensional information, for the analysis of droplet combustion experiments relies on the assumption that the droplets and their flames are volumes of revolution. Only then can a two-dimensional description of the droplet and its flame provide sufficient information to determine their shape and size. This assumption is valid when gas phase spherical symmetry prevails, as is achieved by removing all forms of convection around the droplet, which is accomplished by burning "small" droplets in a low gravity environment (Dietrich *et al.*, 1996; Avedisian, 2000; Bae and Avedisian, 2004; Hicks *et al.*, 2010). Fig. 1a illustrates the resulting configuration. The spherical droplet is concentric with its spherical flame, which in turn is concentric with a soot "shell" that may develop as a result of the formation of particulates during the burning process (the physics of soot shell development is discussed in Jackson and Avedisian (1994), Choi and Kyeong-Okk (1996), Avedisian (1997)). The spherical object is then truly a volume of revolution of the planar circular image. This situation is well suited to the application of an automated image analysis algorithm that can detect an edge of interest (*e.g.*, droplet boundary), determine an effective diameter from it, and advance through a sequence of images.

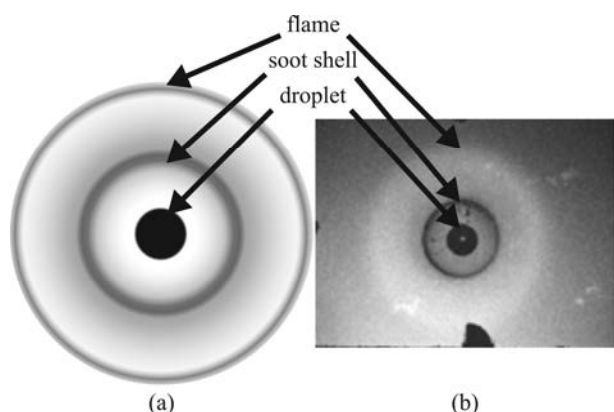


Fig. 1. (a) Idealization and (b) film photo of a spherically symmetric droplet, showing the flame and soot shell (Jackson and Avedisian, 1994).

Figs. 1 to 3 are representative of the images that are encountered in droplet combustion experiments carried out in a low gravity environment. From such images, physical dimensions must be extracted to provide quantitative data of the burning process. Fig. 1b (Jackson and Avedisian, 1994) depicts a free-floating burning droplet from one frame of a sequence for an n-heptane droplet ( $C_7H_{16}$ , boiling point of  $98^\circ C$ ) obtained from a high speed 16 mm LOCAM II movie camera operated at 200 frames per second. Fig. 2 (Liu and Avedisian, 2012) shows 8 images selected from the burning history of an n-heptane droplet as captured with a 3.9 megapixel digital video camera operated at 200 frames per second with the droplet held by two crossed SiC support fibers ( $14\ \mu m$  diameter). The initial diameter of the heptane droplet is 0.52 mm. In all these experiments the droplet is ignited by high voltage sparks formed across two electrode pairs on either side of the droplet. The outer luminous zone in Fig. 1b is the droplet's flame. The horizontal bands in Fig. 2 are support fibers. The thin black circle that develops around the droplet in Fig. 2 is a soot shell. The diameter of the soot shell is of interest because of its relevance to environmental air quality.

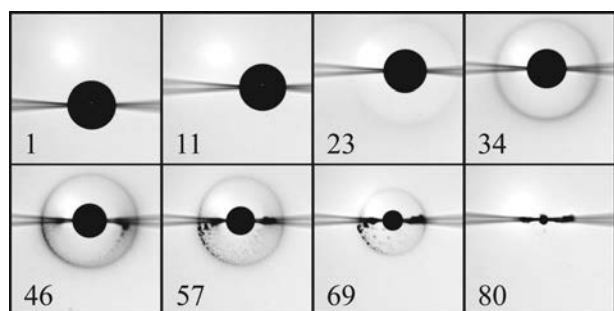


Fig. 2. Selected images from a fiber-supported heptane droplet burning experiment.

Early image processing techniques used for analog films of droplet combustion studies involved first manually digitizing each image using a Vanguard Motion Analyzer and tracing the boundary of the droplet with a digitizing pen on a Thomson plotting table (Stewart *et al.*, 1969; Law and Williams, 1972). This method was also commonly used in studies of the dynamic motions associated with biological activities (Stewart *et al.*, 1969; Carpenter *et al.*, 1983). A variation of this approach for droplet analysis was developed by Choi *et al.* (1988) and Choi (1992). It involved using a micro-processor to detect the droplet boundary from digitized images using mean filtering and intensity thresholding methods. Commercial software now exists to accomplish tasks such as tracking boundaries, measuring diameters, and advancing images in a sequence (*e.g.*, Image-Pro, Image-Warp, CLE-MEX, SigmaScan, and PAX-it, etc.).

There are several issues to consider in the analysis of droplet combustion images. Even though the droplet boundary may be in sharp focus and, accordingly, can be easily detected (*e.g.*, Fig. 2), the soot cloud that surrounds it may obscure parts of the droplet boundary. Fig. 3 shows images selected from a 102-frame sequence of a fiber-supported burning toluene droplet ( $C_7H_8$ , boiling point of  $111^\circ C$ ) with an initial diameter of 0.52 mm. Before ignition (1) the droplet is in sharp focus with high contrast. However, soon into the burning history the soot forms thick and contiguous structures that attach to the fiber and obscure parts of the droplet boundary. An automated analysis routine can theoretically construct a boundary when only part of it is visible (*e.g.*, determining a circle using only a few points on an arc). This task is facilitated, in the case of droplet combustion, by the knowledge that the droplet should ideally have a spherical shape for the experimental conditions that are the focus of the present study.

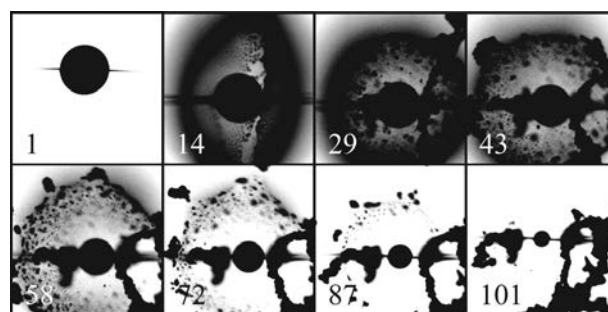


Fig. 3. Image selected from a fiber-supported toluene droplet burning experiment.

In this paper we describe an algorithm for automatically determining the dimensions of droplets when

only partial information about the droplet's boundary is available. We implemented the algorithm in MATLAB and the full program is provided in the "supplementary material" section of the journal. The algorithm is tailored to the case of near-spherical droplet symmetry so that the droplet's cross section can be approximated by a circle or an ellipse.

The paper is organized as follows. The next section reviews a manual approach to the analysis of droplet burning histories using a commercial software package. We then describe the DROPLETD algorithm in detail, and we subsequently compare results of the automated analysis to the manual analysis approach.

### MANUAL DATA ANALYSIS WITH COMMERCIAL SOFTWARE

As a base case for comparison we used the package Image-Pro Plus v.6.3 as our prior droplet burning studies (Bae and Avedisian, 2004; 2009; Liu and Avedisian, 2012) employed this package for image analysis. A typical procedure for manually obtaining droplet diameter measurements includes the following steps: (1) the droplet image is loaded into the software; (2) a threshold value of grayscale intensity is selected to convert the original grayscale image (with intensity values ranging from 0 to 255) into a black and white (black = 0, white = 255) binary image; (3) an elliptical "area of interest" (AOI) tool is activated and the AOI is manually placed on what is perceived to be the droplet boundary based on the assigned threshold value; (4) the pixel readings for the width  $W$  and height  $H$  of the elliptical AOI are recorded; (5) the effective droplet diameter, in units of pixels, is calculated by taking a geometric average of the width and height of the ellipse (*i.e.*,  $D = (W \times H)^{0.5}$ ); and (6) the process is repeated for each frame in the sequence.

The intensity threshold and AOI tool of Image Pro is illustrated in Fig. 4. The points in the red areas have an intensity below the threshold. The grayscale intensity threshold that correctly reveals the droplet boundary may vary from image to image. Image-Pro has an automatic threshold feature that attempts to automatically determine an appropriate intensity threshold. Fig. 4a-1 is taken from the heptane sequence of Fig. 2. For a droplet image with little background noise, such as for heptane, this feature succeeds at differentiating the droplet from a uniform background (Fig. 4a-2). Alternatively, the threshold may be adjusted manually, as is done for Fig. 4a-3 and Fig. 4a-4. Fig. 4a-3 shows the result of a threshold of 20, which poorly distinguishes the droplet from its surroundings. Fig. 4a-4, on the other hand, shows the success of a

threshold of 160. Ideally the threshold value should generate a region that just blocks the droplet but does not cover the actual droplet boundary. Fig. 4a-5 shows that after a threshold is chosen, whether automatically or manually, Image-Pro converts the droplet image into a black and white image. Fig. 4a-6 shows a manual fitting of an AOI, represented by the dashed line, to the droplet boundary that is now clearly evident in the black and white image.

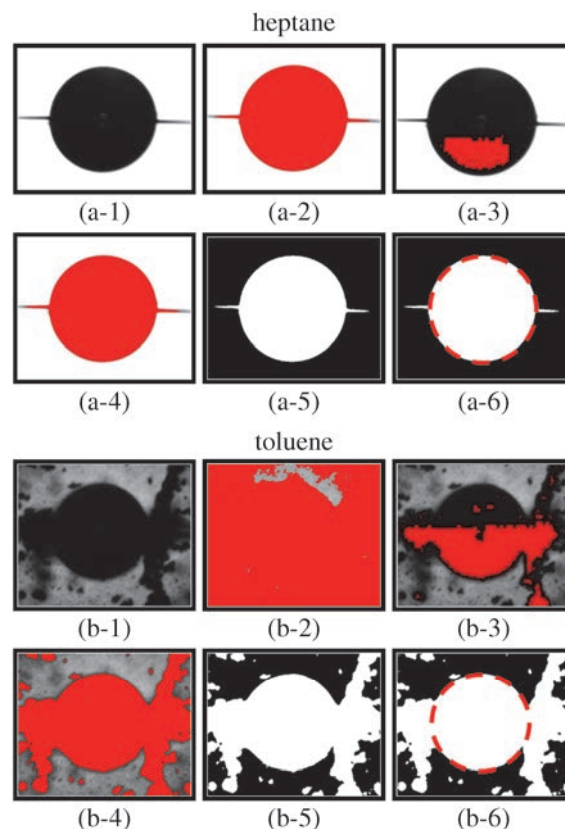


Fig. 4. Steps in a manual Image-Pro analysis, for both heptane and toluene droplets.

Fig. 4b-1 through Fig. 4b-6 illustrate the challenge of applying the same procedure to a droplet image with considerable background noise from soot formation, in this case from the toluene sequence of Fig. 3. The original image is shown in Fig. 4b-1. Fig. 4b-2 shows the result of using Image-Pro's automatic threshold feature to distinguish the droplet from its surroundings. Clearly, the automatic threshold feature is not successful. In this case, the user must find a threshold manually. Fig. 4b-3 and Fig. 4b-4 show the results of two different thresholds found manually. The threshold used in Fig. 4b-4 satisfactorily distinguishes the droplet from its surroundings. Fig. 4b-5 shows an AOI that is sized with some operator jud-

gment to manage the irrelevant information of the fiber support and soot surrounding the droplet.

The procedure outlined above provides droplet diameters in units of pixels, which must be converted to physical units (*e.g.*, millimeters). The conversion is accomplished using a conversion factor obtained from the analysis of an image of a calibration ball (a 0.79 mm tungsten carbide ball bearing) that is recorded under the same lighting conditions and with the same focal distance as are used for the droplet images. Since the correct intensity threshold may vary from image to image, it would seem that the conversion factor may also vary from image to image. However, in the calibration image the ball is so opaque and the ball's boundary is so sharp that the entire range of intensity threshold values that is relevant in the analysis of droplet images yield the same conversion factor. Therefore, the calibration factor is conveniently independent of intensity threshold in the range that is relevant.

The above steps are often laborious and time-consuming when analyzing many images (*e.g.*, analyses can take several hours for a 100-frame sequence). In the next section we describe an algorithm that automates these steps.

### THE MATLAB ALGORITHM: DROPLETD

An algorithm termed "DROPLETD" is described by the flowchart in Fig. 5, and a MATLAB implementation of the algorithm is provided as supplementary material. The algorithm consists primarily of two operations: edge detection and shape fitting. The edge detection step provides a collection of candidate boundary points that may be on the droplet boundary and to which an assumed droplet shape may be fit. In the shape fitting step, a shape is fit to the candidate boundary points in order to obtain an effective diameter of the droplet, which is the quantity desired from each image. Candidate boundary points are iteratively removed from the collection of candidate boundary points until the resulting fit provides an effective droplet diameter that falls below a specified error bound.

Edge detection may be performed in one of two ways: with a constant intensity threshold; or with an adaptive intensity threshold. Edge detection is described in detail later in this section. The shape fitting process is also performed in one of two ways: as a circle fit or as an ellipse fit. Furthermore, there are two different methods by which a circle or ellipse can be fit to the boundary points: the so-called "point sampling" (PS) method or the "global least squares" (GLS) method. In this implementation, circle fits are

tied to the PS method, and ellipse fits are tied to the GLS method for reasons discussed later. The shape fitting methods are described further in the Appendix.

The algorithm starts by displaying to the user the first image in the sequence of images. The user selects a point on the interior of the droplet to specify the center of a region of interest (ROI). The ROI is a square with side length  $2s$  in which the algorithm will search for droplet boundary points. The value of  $s$  for the first image in the sequence,  $s_1$ , is a parameter of the algorithm. In the present study, a value of 300 pixels is used for  $s_1$ , which was found to work well for droplets whose initial diameter is about 250 pixels. For all subsequent images,  $s$  is set to be slightly larger than the diameter computed for the droplet in the previous image. A key aspect of the automated nature of this algorithm is that for all frames after the first, it is not necessary for the user to specify the center of the ROI. Instead, the center of the ROI for subsequent images is taken to be the center of the droplet in the previous image. For the algorithm to function properly, the center of the ROI must be within the droplet boundary, and  $s$  must always be larger than the droplet's radius. Thus, the droplet in one frame is allowed to have a displacement from its location in the previous frame of about  $2s$  in order for the center of the ROI to remain within the droplet boundary.

The edge detection method used in the algorithm is an intensity threshold method in which a grayscale image is converted into a black and white image with the use of a grayscale intensity threshold,  $I_t$ . Then, a collection of boundary points is created from the points in the ROI, when scanning from the center of the droplet outwards, at which the color transitions from black to white.

The constant intensity threshold method operates by using a single value of  $I_t$  for all images in the sequence. The appropriate value for a sequence depends on the fuel being studied and on lighting conditions. For an adaptive intensity threshold,  $I_t$  is calculated for each image using data from the previous image in the sequence. The value of  $I_t$  is found to be proportional to the average intensity value of certain points across the droplet and its surroundings. Three scan lines that are 45 degrees apart and across the droplet center (shown in Fig. 6) are used to sample the intensity values for the droplet and the background. While more scan lines could be used to compute the adaptive intensity threshold, the use of three scan lines was found to be sufficient for obtaining accurate results. It is important, however, that none of the scan lines are aligned with the support fiber, as this would incorrectly decrease the value computed for  $I_t$ .

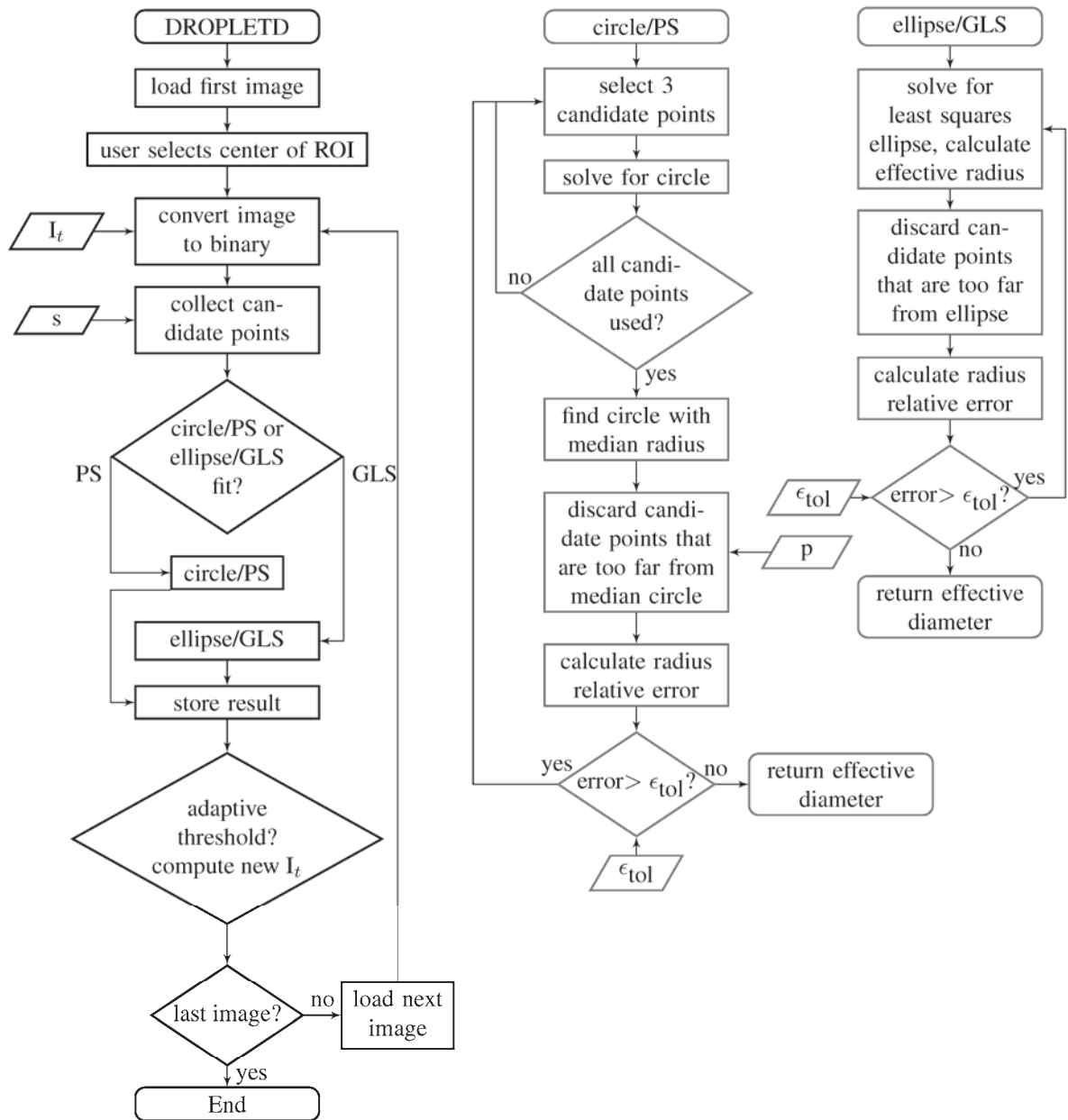


Fig. 5. Flowchart for the DROPLETD automated analysis.

In order to weight the droplet and its boundary equally in this averaging, the scan lines have a length that is twice the diameter of the droplet from the previous image. The average intensity value of these sampled points is then used to determine  $I_t$ ,

$$I_t = f \frac{\sum_k I_k}{N}, \quad (1)$$

where  $f$  is a proportionality constant,  $I_k$  is the intensity of the  $k$ -th point along the three scan lines, and  $N$  is the total number of points along all three scan lines. The threshold defined by Eq. 1 is applied to the next

image in the sequence.

The value for  $f$  depends on the fuel being studied and on lighting conditions, as well as on other parts of the algorithm (e.g., the shape fitting method used). A small value for  $f$  favors a darker threshold and thus tends to underestimate the droplet diameter, and is accordingly appropriate for droplets with bright surroundings. In the present study, values for  $f$  were selected by examining the values that generally minimize the error between DRPOLETD and a manual analysis. It was found that the error reached a minimum plateau for  $0.67 < f < 1.0$ .

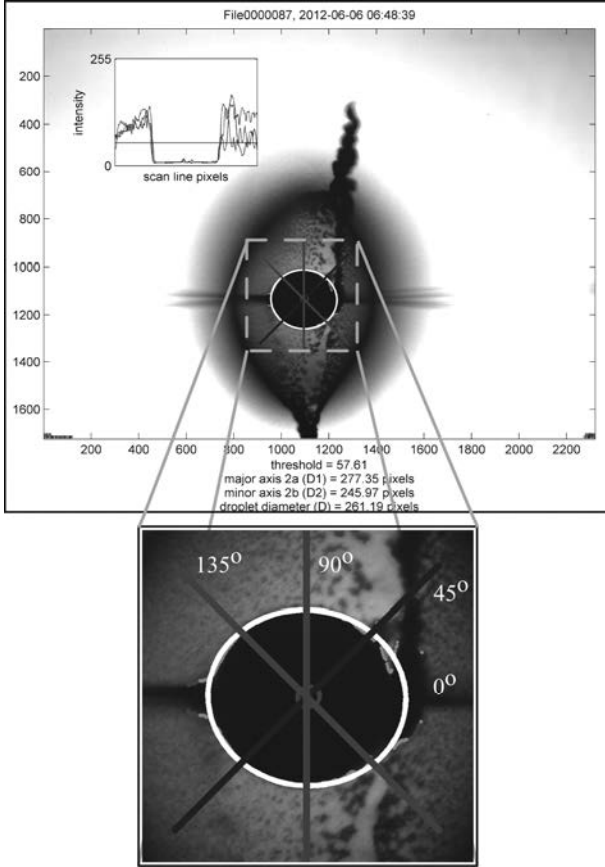


Fig. 6. Output of DROPLETD analysis of the 15th frame of the toluene experiment.

Two other edge detection methods were also explored. The first of these is a “gradient” threshold method in which the gradient of the grayscale intensity determines the droplet boundary (*i.e.*, inflection point). Thus, a collection of candidate boundary points could potentially be gathered from the points at which the gradient of the intensity exceeds some threshold. This method, however, typically overestimates droplet diameters. Edge following methods, which attempt to follow a trail of high gradient values (Pitas, 2006), were also considered. However, such methods were derailed by the presence of the support fiber and were not considered further.

Once equipped with a collection of candidate boundary points, the algorithm fits a shape to the boundary points in an attempt to determine the droplet’s effective radius or diameter. The details of the procedure to fit a prescribed shape (circle or ellipse) to the boundary points are discussed in the Appendix. In the case of an ellipse fit, the effective droplet radius is the geometric mean of the fitted ellipse’s semi-major and semi-minor axis lengths.

In a typical analysis, a fraction of the candidate

boundary points are fairly distant from the actual droplet boundary. In order to obtain accurate results, it is important that these points are discarded and that a new fit is performed with only the remaining candidate boundary points. This is especially important when the presence of a large amount of soot causes the algorithm to incorrectly detect the boundary of the soot to be boundary of the droplet. This iteration continues until the effective droplet radius falls below a specified error bound.

The discarding of boundary points is controlled with an iterative process whereby points satisfying

$$\frac{|\Delta_i - r_i|}{r_i} > p, \quad (2)$$

are discarded, where  $\Delta_i$  is the distance between the boundary point and the center of the droplet and  $r_i$  is the radius of the circle fit in the  $i$ -th iteration. In the present study,  $p = 0.1$  is used (*i.e.*, the distance between the boundary point and the center of the circle fit must be within 10% of  $r_i$  to survive an iteration). For ellipse fits, any candidate boundary point that satisfies

$$\Delta_i > (1 + p) a \quad (3)$$

or

$$\Delta_i < (1 - p) b, \quad (4)$$

is discarded, where “a” is the ellipse’s semi-major axis length, “b” is the ellipse’s semi-minor axis length. A new fit is found with the remaining boundary points, and a new radius  $r_{i+1}$  is computed. This process continues until the condition

$$\frac{|r_{i+1} - r_i|}{r_{i+1}} < \epsilon_{\text{tol}}, \quad (5)$$

is met, where a value of  $10^{-4}$  for  $\epsilon_{\text{tol}}$  has been used in the present study. The method typically requires 2 to 15 iterations for the error to fall below this tolerance. This procedure is performed for each image in the sequence to provide a history of the effective droplet diameter. A summary of the parameters that control the operation of DROPLETD is given in Table 1.

As with the manual analysis, the droplet diameters computed by the algorithm are in units of pixels. In order to obtain the diameter of the droplet in physical units, a conversion factor must be obtained by using DROPLETD to analyze a calibration image using the same edge detection and shape fitting methods used for the droplet images.

Table 1. *The parameters that control the operation of DROPLETD, and their default values.*

Parameter	Description	Default
$s_1$	Half the side length of the region of interest for edge detection (in pixels).	300
$I_t$	Grayscale intensity threshold (integer between 0 and 255). More relevant for a constant threshold.	100
$\epsilon_{tol}$	Error tolerance for the convergence on a droplet's radius.	$10^{-4}$
$p$	Controls how candidate points are discarded. A larger value is more allowing.	0.1
$f$	Proportionality constant in the calculation of the adaptive intensity threshold.	1.0

The user can choose which of the two edge detection or shape fitting methods to use. The choice of which of these methods to use depends on the nature of the burning sequence. For fuels that generate minimal soot, a constant intensity threshold was found to give accurate droplet diameter results. However, for fuels that generate so much soot that the surrounding intensity changes throughout the burning, an adaptive intensity threshold is often necessary. The determination of whether a circle fit or an ellipse fit is more appropriate is not as straightforward, though a circle fit can be more resilient in cases where soot blocks part of the droplet's boundary.

## RESULTS AND DISCUSSIONS

In this section, we present comparisons between the automated (DROPLETD) and manual (Image-Pro) analysis of droplet combustion experiments. We employ the heptane and toluene burning sequences of Figs. 2 and 3, respectively, for these comparisons. The DROPLETD results are compared to the Image-Pro results for a variety of the options available in DROPLETD. These include the use of a constant or adaptive intensity threshold, selecting the value of  $f$  (Eq. 1), imposing circle or ellipse fits to the droplet shape, and considering the effect of the PS or GLS methods for using boundary points to obtain a fit.

The success of the automated analysis is judged with figures that display the evolution of the square of droplet diameter,  $D^2$ , based on the classical theory of droplet combustion (Turns, 2006). From this theory, the evolution of  $D^2$  is predicted to be linear though in practice this is often not the case (Liu and Avedisian, 2012). The difference between  $D$  obtained from the automated analysis algorithm presented here ( $D_{auto}$ ) and the manual ( $D_{man}$ ) analysis for each frame in a sequence is defined as

$$\epsilon = \frac{D_{auto} - D_{man}}{D_{man}}. \quad (6)$$

A negative error indicates that DROPLETD underestimated the  $D$  relative to the  $D_{man}$ . The output from DROPLETD is converted to physical units (*e.g.*, mm) as discussed in the previous section.

Fig. 7 compares various DROPLETD analyses with an Image-Pro analysis for heptane. The images were analyzed in four ways: a circle fit to the droplet shape using the PS method and an ellipse fit to the droplet shape using the GLS method, for both adaptive and constant thresholds. For the adaptive threshold,  $f = 1.0$  in Eq. 1 was used. Fig. 7a shows that all four methods successfully approximate the evolution of  $D^2$  from the manual analysis. Note that the total time for DROPLETD to complete the automated analyses for around 100 consecutive images is less than 3 min (with a 3.1 GHz Intel Core i5-2400 CPU), compared to nearly 150 min needed for manual analyses for the same set of images. Only data for every fourth frame are shown in Fig. 7a to avoid clutter. An adaptive threshold with an ellipse fit is the only method that overestimates the droplet's diameter, as this method is able to accommodate more distant candidate boundary points. The maximum relative error consistently occurs at the end of the burning because the thickness of the droplet boundary becomes relatively large compared to the smaller droplet at the end of burning, and a larger fraction of the boundary is obscured by the support fiber and surrounding soot. Fig. 7b shows the evolution of the error (Eq. 6) for every other image in the sequence. After frame 40 the constant method underestimates the droplet diameters. Holding the threshold constant does not provide for an adaptation to the slightly changing surrounding intensity as the soot shell forms and evolves. An adaptive intensity threshold corrects for this effect. A value for  $f$  of 1.0 with the adaptive threshold reduces the error by a factor of approximately two compared to the use of  $f = 0.67$ . For both types of thresholds for heptane, the ellipse fit is more successful than the circle fit because it is more adaptive to the droplet's shape: the average eccentricity of the ellipses is about 0.32.

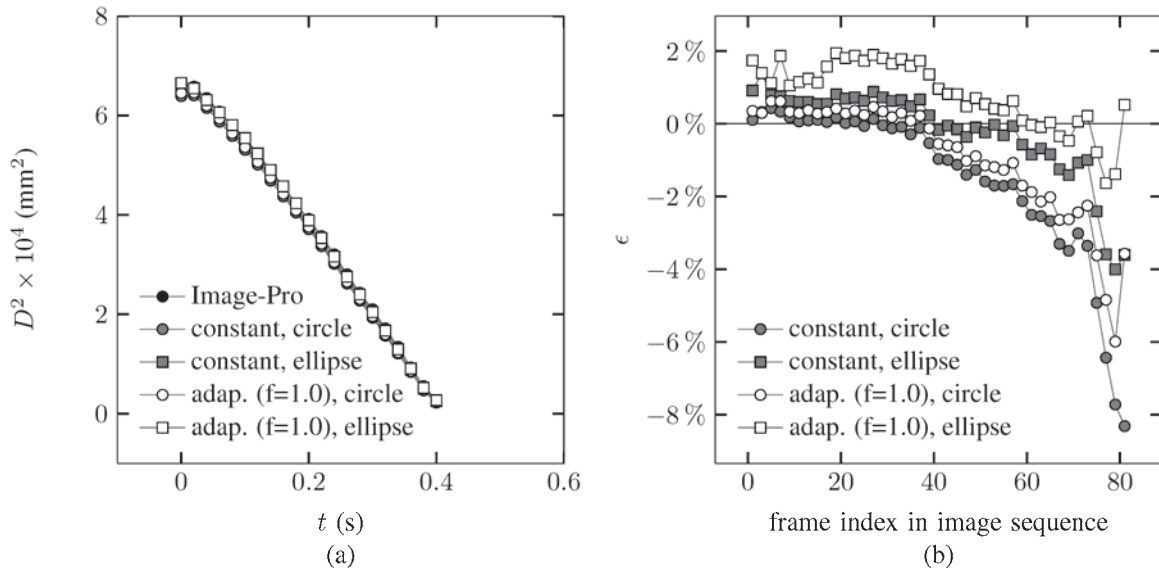


Fig. 7. Evolution of (a)  $D^2$  and (b) error (Eq. 6) for heptane (cf. Fig. 2).

Fig. 8 compares the evolution of  $D^2$  for toluene obtained using constant and adaptive thresholds (and with the PS method for a circle fit and the GLS method for the ellipse fit to the droplet shape). Fig. 8a with  $f=1$  shows that for  $t < 0.25$  s, the automated analysis results using a constant threshold deviate substantially from the manual analysis results. This initial difference is attributed to excessive soot formation that, compared to the heptane experiment, produces a more pronounced change in the surrounding

intensity early in the burning process. A constant threshold cannot adapt to such changes in surrounding intensity, and such an analysis does not succeed at reproducing the results obtained with Image-Pro. An adaptive threshold is necessary for these images. For  $t > 0.25$  s all four analyses are consistent. Fig. 8b compares the relative errors for the adaptive threshold method for toluene for two different values of  $f$ . The results show that  $f=1.0$  produces a smaller error compared to  $f=0.67$ , as the larger value provides a looser fit.

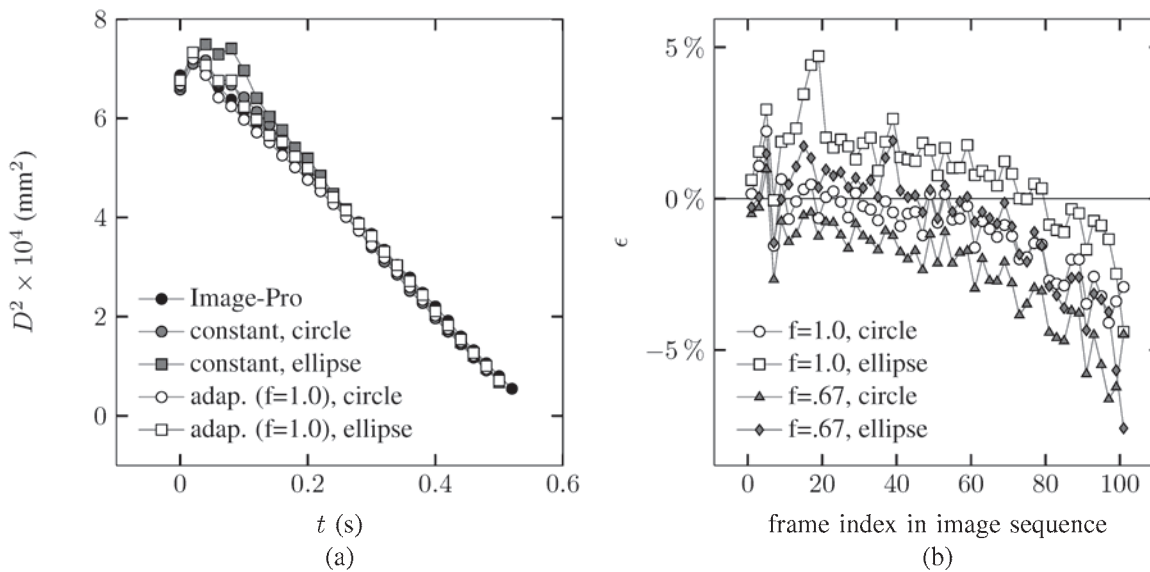


Fig. 8. Evolution of (a)  $D^2$  and (b) error (Eq. 6) for toluene (cf. Fig. 3).

The results of two adaptive threshold analyses for toluene are shown in Fig. 9 using the GLS method of detecting boundary points. In this case, the droplet shape is assumed to be a circle, though this combination is not an option in the distributed version of the algorithm (for reasons explained here). Results for  $f = 0.67$  and  $f = 1.0$  are compared. The results show significant divergence of the droplet diameter for  $t > 0.2$  s which also coincides with a large amount of soot forming on the support fiber that blocked a portion of the droplet boundary (*i.e.*, the impact of the fiber on sooting configuration was discussed in Avedisian and Jackson (2000)). The GLS method in combination with a circle fit is too accommodating to erroneous boundary points from soot, and the algorithm incorrectly determines  $D$ . This result motivates tying the circle fit for the droplet shape to the PS method instead of the GLS method. By changing  $f$  from 1.0 to the smaller value of 0.67, the algorithm detects the candidate boundary points to be closer to the dark center of the droplet.

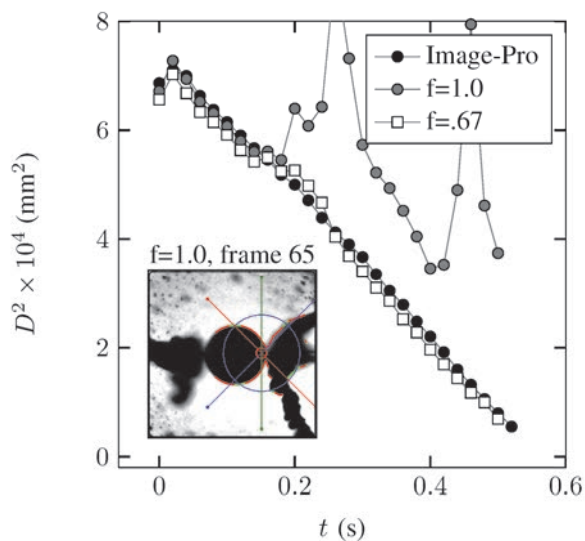


Fig. 9. Evolution of  $D^2$  plot for toluene using circle fits with the GLS method.

As is evident in Figs. 7 to 9 the automated method tends to underestimate the droplet diameter. This effect is less noticeable when plotting  $(D/D_0)^2$  versus  $t/D_0^2$  as per the classical theory of droplet burning (Turns, 2006). In these coordinates, constant differences across methods are suppressed.

Fig. 10 summarizes the automated analysis of a representative frame of the toluene burning history (*cf.* Fig. 3) for a variety of settings. The white curve is the shape that is finally fitted to the droplet, the red dots are candidate boundary points that were discarded, and the green dots are points that are used in the final

fit. A constant  $I_t$  leads to the creation of an initial collection of candidate boundary points that are too far from the droplet boundary. In subsequent iterations, these points are discarded from the collection. However, with an ellipse fit, enough of these points remain in the collection that the resulting ellipse is clearly too large. This corresponds to the initial large error seen in Fig. 8a for the constant ellipse analysis. Fig. 10 also shows that an adaptive threshold prevents the algorithm from considering points far from the droplet boundary, but that an ellipse can be more accommodating to boundary points that actually belong to soot.

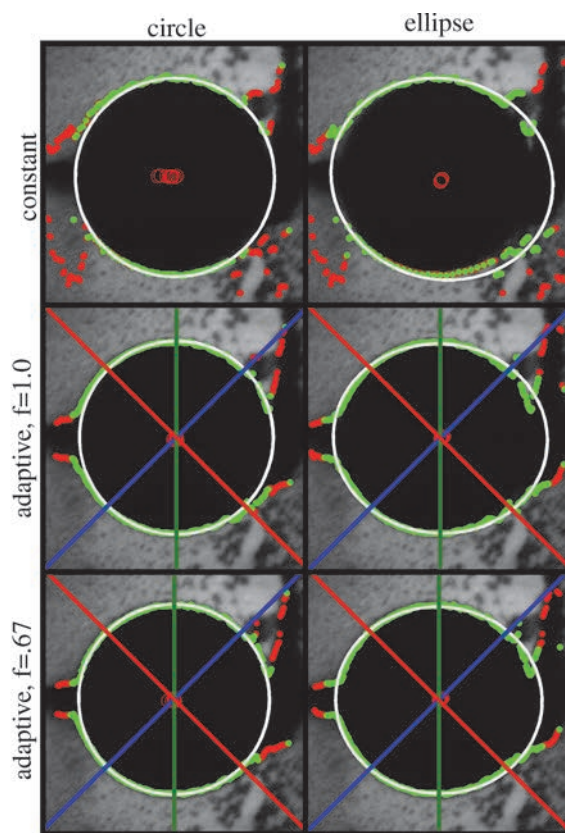


Fig. 10. Comparison of edge detection and shape fitting settings for the 15<sup>th</sup> frame of the toluene burning sequence from Fig. 3.

## CONCLUDING REMARKS

An algorithm has been described that successfully extracts droplet diameters from digital images of burning droplets of sooting fuels in an automated manner with minimal error. This results in a saving of time in the analysis process by almost a factor of fifty compared to the typical manual method of analysis.

The proper selection of the various options in the algorithm depends on the nature of the data being

analyzed. For images with low noise or less soot (e.g., heptane), a constant intensity threshold is sufficient for analysis. For fuels in which the droplet's surroundings are changing due to soot formation (e.g., toluene), an adaptive intensity threshold is necessary. Generally,  $f = 1.0$  provides more accurate results compared to setting  $f = 0.67$ . However, under certain conditions a lower value of  $f$  can prevent the algorithm from diverging. Additionally, a circle fit is often preferred instead of an ellipse fit if the droplet boundary is blocked by the formation of large amounts of soot.

## ACKNOWLEDGMENT

This work was supported in part by the National Aeronautics and Space Administration grant number NNX08AI51G (Mr. Michael Hicks, Project Monitor) and the New York State Space Grant Consortium to Cornell University.

## REFERENCES

- Avedisian CT (1997). Soot formation in spherically symmetric droplet combustion, in physical and chemical aspects of combustion. Gordon and Breach Publ., Chapter 6, pp. 135–60.
- Avedisian CT, Yang JC, Wang CH (1988). On low-gravity droplet combustion. Proceedings of the Royal Society of London A 420:183–200.
- Avedisian CT (2000). Recent advances in soot formation from spherical droplet flames at atmospheric pressure. *J Prop Power* 16:628–56.
- Avedisian CT, Jackson GS (2000). Soot patterns around suspended n-Heptane droplet flames in a convection-free environment. *J Prop Power* 16:974–9.
- Bae JH, Avedisian CT (2004). Experimental study of the combustion dynamics of jet fuel droplets with additives in the absence of convection. *Combustion and Flame* 137:148–62.
- Bae JH, Avedisian CT (2009). Nonane droplet combustion with and without buoyant convection: flame structure, burning rate, and extinction in air and helium. Proceedings of the Combustion Institute 32:2231–8.
- Carpenter GC, Duvall D (1983) How-To-Do-It: Motion Picture and Videotape Analysis of Behavior. *The American Biology Teacher* 45:349–52.
- Choi MY (1992). Droplet Combustion Characteristics under Microgravity and Normal-Gravity Conditions, Ph.D Thesis, Department of Mechanical and Aerospace Engineering, Princeton University, Princeton, N.J.
- Choi MY, Dryer FL, Haggard, Jr. JB, Brace MH (1988), Further Observations on Microgravity Droplet Combustion in the NASA-Lewis Drop Tower Facilities: A Digital Processing Technique for Droplet Burning Data. AIP Conference Proceedings 197:338–61.
- Choi MY, Kyeong-Okk L (1996). Investigation of Sooting in Microgravity Droplet Combustion. *Proc Comb Inst* 26:1243–9.
- CLEMEX intelligent microscopy, <[www.clemex.com](http://www.clemex.com)>.
- Dietrich DL, Haggard Jr. JB, Dryer FL, Nayagam V, Shaw BD, Williams FA (1996). Droplet Combustion Experiments in Spacelab. *Proc. Comb. Inst.* 26:1201–7.
- Fitzgibbon A, Pilu M, Fisher R (1999). Direct Least Squares Fitting of Ellipses. *IEEE Trans Pattern Anal Mach Intell* 21:476–80.
- Gander W, Golub GH, Strebler R (1994). Least-Squares Fitting of Circles and Ellipses. *BIT* 43:558–78.
- Halir R, Flusser J (1998). Numerically Stable Direct Least Squares Fitting of Ellipses. *Proc. WSCG'98*:125–32.
- Hendel T (2010). <<http://www.mathworks.com/matlabcentral/fileexchange/22423-ellipse-fit>>, 18 May 2010.
- Hicks MC, Nayagam V, Williams FA (2010). Methanol droplet extinction in carbon-dioxide-enriched environments in microgravity. *Combustion and Flame* 157: 1439–45.
- Image-Pro Plus Version 6.3 for Windows Start-Up Guide (2008). Media Cybernetics, Inc., Bethesda, MD.
- ImageWarp, <[www.imagewarp.com](http://www.imagewarp.com)>.
- Jackson GS, Avedisian CT (1994). The Effect of Initial Diameter in Spherically Symmetric Droplet Combustion of Sooting Fuels. Proceedings of the Royal Society of London A 446:255–76.
- Law CK, Williams FA (1972). Kinetics and Convection in the Combustion of Alkane Droplets, *Combustion and Flame* 19:393–405.
- Liu YC, Avedisian CT (2012) A Comparison of the Burning Characteristics of Sub-millimeter Droplets of Binary Mixtures of iso-Octane, n-Heptane and Toluene with a Commercial Unleaded Gasoline, *Combustion and Flame* 159:770–83.
- PAX-it Image Database Software, <<http://www.paxit.com/index.asp>>.
- Pitas I (2006), Digital image processing algorithms and applications, John Wiley & Sons, New York, New York.
- SigmaScan, Systat Software Inc., <[www.sigmaplot.com/index.php](http://www.sigmaplot.com/index.php)>.
- Stewart GH, Lynch PR, Gimenez JL (1969). Technical Note: Versatile Technique for the Analysis of Dynamics Multi-dimensional information. *Medical and Biological Engineering and Computing* 7:435–8.
- Turns SR (2006), An Introduction to Combustion, 2<sup>nd</sup> ed., McGraw Hill, Boston, M.A., p. 378.
- Weisstein EW, "Ellipse." From *MathWorld*—A Wolfram Web Resource. <<http://mathworld.wolfram.com/Ellipse.html>>

## APPENDIX

This section describes the methods used to fit a collection of points to a circle or ellipse. The objective of fitting a circle or ellipse to the collection of points is to obtain the effective diameter of the shape that the points describe. The use of an ellipse fit is considered since it is a more general shape and the shape of a droplet's cross-section may deviate from a circle due to motion of the droplet at the start of its free fall, and disturbance from the spark at the time of ignition. An effective droplet diameter is calculated as the geometric mean of the ellipse's major and minor axis lengths. The choice of whether to use a circle or ellipse depends on the burning sequence. Indeed, the presence of soot in the images sometimes derails an ellipse fit, and a circle fit is more appropriate in such cases.

There are two ways by which the algorithm can use its collection of candidate boundary points to obtain a circle or ellipse that approximates the candidate boundary points. The first of these is the "point-sampling" (PS) method, which operates by generating many different exact fits and choosing the one with an effective radius closest to the mean effective radius from all the fits. The second of these is the global least squares (GLS) method, which generates a single approximate fit to obtain an effective radius. In practice, circle fits are more successful with the PS method, and ellipse fits are more successful with the GLS method (*cf.* Fig. 12). Therefore, the PS method is presented only in the context of circle fits, and the GLS method is presented only in the context of ellipse fits.

The first step in the PS method is to divide the collection of candidate points into three groups, as labeled by the Roman numerals I, II, and III in Fig. 11. Then, the algorithm selects the first point from each of these groups and finds the circle that contains them. This requires the solution of the simultaneous equations

$$\begin{aligned} (x_1 - x_c)^2 + (y_1 - y_c)^2 &= r^2 \\ (x_2 - x_c)^2 + (y_2 - y_c)^2 &= r^2, \\ (x_3 - x_c)^2 + (y_3 - y_c)^2 &= r^2 \end{aligned} \quad (7)$$

for the terms  $x_c$ ,  $y_c$ , and  $r$ . The points  $(x_1, y_1)$ ,  $(x_2, y_2)$ , and  $(x_3, y_3)$  represent the points taken from group I, II, and III, respectively. The solution to the set of equations above provides an exact circle fit to these three points. The algorithm creates an array of such circles by moving sequentially through the groups in this manner, as illustrated in Fig. 11. The circle with the median radius is used to represent the droplet boundary.

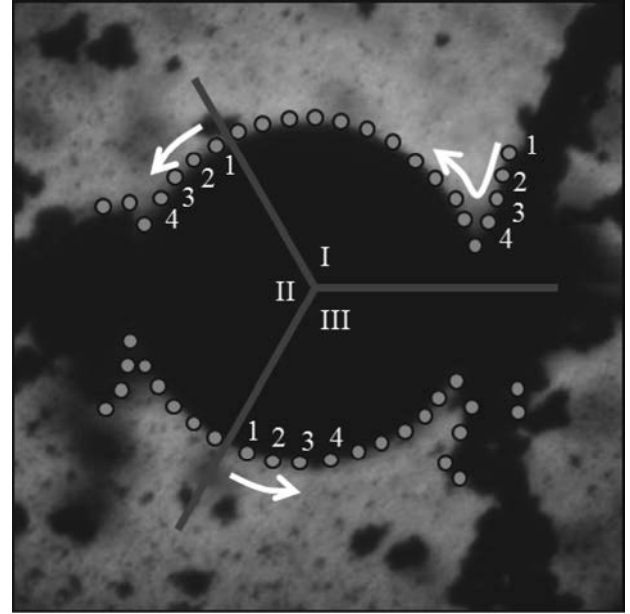


Fig. 11. Illustration of the point sampling (PS) method for circle fits.

The GLS method determines the ellipse that best fits the collection of all candidate points in a least-squares sense. The equation for an ellipse can be expressed as

$$x^2 + c_1xy + c_2y^2 + c_3x + c_4y + c_5 = 0. \quad (8)$$

If an ellipse is to be fit to only five points, a set of five equations of the form of Eq. 8 can be solved simultaneously to obtain the coefficients  $c_1$  through  $c_5$  that describe this ellipse. If an ellipse is to be fit to  $N > 5$  points, the system of equations in Eq. 9 must be solved.

$$\begin{bmatrix} x_1y_1 & y_1^2 & x_1 & y_1 & 1 \\ x_2y_2 & y_2^2 & x_2 & y_2 & 1 \\ \vdots & \vdots & \vdots & \vdots & \vdots \\ x_Ny_N & y_N^2 & x_N & y_N & 1 \end{bmatrix} \begin{bmatrix} c_1 \\ c_2 \\ c_3 \\ c_4 \\ c_5 \end{bmatrix} = \begin{bmatrix} x_1^2 \\ x_2^2 \\ \vdots \\ x_N^2 \end{bmatrix}, \quad (9)$$

where  $(x_i, y_i)$  ( $i = 1$  to  $N$ ) represents a candidate point. This set of equations is solved in a least squares sense to determine the values of  $c_1$  through  $c_5$  that can then be used to obtain the center  $(x_{ce}, y_{ce})$  and effective radius  $r_e$  of the ellipse (Hendel, 2010, Weisstein).

The coordinates for the center of the ellipse are

$$x_{ce} = \frac{c_2c_1 - c_1c_4}{c_1^2 - c_2} \quad (10)$$

and

$$y_{ce} = \frac{c_4 - c_1 c_3}{c_1^2 - c_2}. \quad (11)$$

The effective radius of the ellipse is  $r_e = \sqrt{ab}$ , where  $a$  and  $b$  are the semi-major and semi-minor axis lengths given by Eq. 12 and Eq. 13.

$$a = \sqrt{\frac{2(c_4^2 + c_2 c_3^2 + c_5 c_1^2 - 2c_1 c_3 c_4 - c_2 c_5)}{(c_1^2 - c_2)[\sqrt{(1 - c_2)^2 + 4c_1^2} - (1 + c_2)]}}, \quad (12)$$

$$b = \sqrt{\frac{2(c_4^2 + c_2 c_3^2 + c_5 c_1^2 - 2c_1 c_3 c_4 - c_2 c_5)}{(c_1^2 - c_2)[-\sqrt{(1 - c_2)^2 + 4c_1^2} - (1 + c_2)]}}. \quad (13)$$

The PS method is not used with ellipse fits for the following reason. Since an ellipse is defined by five points, the PS method would require the candidate boundary points to be divided into five groups. It is possible, however, that an entire fifth of the droplet boundary is disrupted by the presence of soot. Thus, dividing the boundary points into so many groups can introduce large errors.

Fig. 12 summarizes the various shape fitting options using the candidate boundary points that were detected for the 19th frame of the toluene burning sequence of Fig. 3. Most of the candidate boundary points on the right side of these figures come from soot and not the droplet boundary. Fig. 12a compares circle and ellipse fits with both the PS and the GLS methods. It is evident from this figure that the circle fit does not work well with the GLS method, as the fit is too susceptible to the boundary points on the soot. The circle fit with the PS method, on the other hand, succeeds at avoiding those points. The ellipse fit is also too accommodating to the boundary points on the soot. Thus, one must be careful when using an ellipse fit. For the ellipse fit, there is a slight difference between the PS and GLS methods; most notably the GLS method provides a less eccentric fit. For this reason, the ellipse fit is tied to the GLS method. Fig. 12b compares various other ellipse fits using the GLS method, (*i.e.*, solving Eq. 9) as given by the formulations of Hendel (2010), Halir and Flusser (1998), and Fitzgibbon *et al.* (1999). As the Hendel fit is slightly less eccentric than the others, the DROPLETD algorithm implements Hendel's formulation.

## NOMENCLATURE

AOI: square area of interest defining the droplet  
 $a$ : length of the semi-major axis of an ellipse  
 $b$ : length of the semi-minor axis of an ellipse  
 $I_k$ : grayscale intensity value of point  $k$  (ranging from 0 to 255)

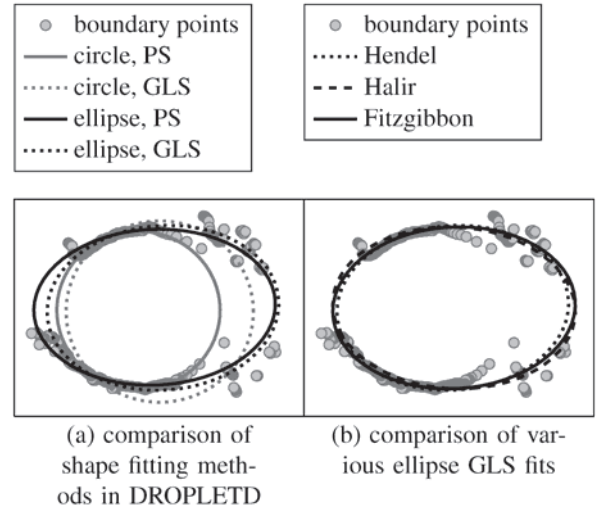


Fig. 12. Comparison of various shape fitting methods for the 19th frame of the toluene droplet burning sequence of Fig. 3.

- $I_t$ : grayscale intensity threshold
- $c_i$ : coefficients in equation for an ellipse
- $D$ : instantaneous droplet diameter (mm)
- GLS: global least square method
- $N$ : number of points along adaptive threshold scan lines
- PS: point sampling method
- $r$ : radius of a circle
- ROI: region of interest for droplet boundary points
- $s$ : half the side length, in pixels, of the ROI square
- $t$ : time (s)
- $x$ : x coordinate of a candidate boundary point
- $y$ : y coordinate of a candidate boundary point
- $f$ : proportionality constant for adaptive intensity threshold
- $\Delta$ : distance from a boundary point to the estimated center of a droplet
- $p$ : parameter controlling the discarding of candidate boundary points

### Greek symbols:

- $\varepsilon$ : relative error between the automated and manual analyses
- $\varepsilon_{tol}$ : error tolerance for shape fitting iterations

### Subscripts:

- auto: automated analysis done by DROPLETD
- man: manual analysis done with Image-Pro
- $c$ : center of a circle
- ce: center of an ellipse
- $i$ :  $i$ -th boundary point in a collection of candidate boundary points